Level structure of ^{92}Mo at high angular momentum: Evidence for $Z=38$, $N=50$ core excitation

N. S. Pattabiraman, S. N. Chintalapudi, and S. S. Ghugre
Inter University Consortium For DAE Facilities, Calcutta Centre, Sector III LB-8, Bidhan Nagar, Kolkata 700 098, India

B. V. Tirumala Rao, M. L. N. Raju, and T. Seshi Reddy
Department of Nuclear Physics, Andhra University, Visakhapatnam 530 003, India

P. K. Joshi, R. Palit, and H. C. Jain
Tata Institute of Fundamental Research, Dr Homi Babha Road, Mumbai 400 005, India
(Received 13 July 2001; published 3 April 2002)

In-beam γ-ray spectroscopic studies of the $N=50$ nucleus ^{92}Mo, up to spins of $J\sim 18\hbar$ and $E_x \sim 12$ MeV, are reported using a heavy ion fusion reaction with a ^{28}Si beam at an incident energy of 138 MeV on an isotopically enriched ^{74}Ge target. Sixteen new transitions belonging to this nucleus have been observed and placed in the decay scheme using the conventional γ-γ coincidence data. The level scheme derived from these measurements is compared with shell model calculations. The presence of gamma rays with $E_\gamma \sim 2$ MeV at $J\sim 14\hbar$ is indicative of the breaking of the $N=50$ core. The occurrence of gamma rays with $E_\gamma \sim 2$ MeV at low spins ($J\sim 8\hbar$) indicates the excitation of protons across the $Z=38$ core. This is supported by large-basis shell model calculations. The deduced level scheme exhibits single-particle behavior up to the highest observed spins and excitation energies.

DOI: 10.1103/PhysRevC.65.044324 PACS number(s): 27.60.+j, 23.20.Lv, 23.20.En, 21.60.Cs

I. INTRODUCTION

The present work is a part of an attempt to systematically study the level structure at high angular momentum of nuclei in the vicinity of $N=50$ shell closure. The nuclei in this region have attracted theorists and experimentalists since the early days of the shell model. The advent of modern gamma arrays and the heavy ion beams readily available from accelerators have made it possible to study these nuclei under extreme conditions of rotation [1–3].

The low-lying levels of these nuclei are well described within the spherical shell model framework using an inert neutron core and protons within the $f_{5/2}, p_{3/2}, p_{1/2}, g_{9/2}$ orbitals [4]. However, higher-angular-momentum states are dominated by the excitation of a single $g_{9/2}$ neutron across the $N=50$ shell closure, into the next oscillator shell [5,6].

The present study extends these investigations to the vicinity of the $Z=38$, 40 semimagic shell closures. Nuclei with $Z\sim 40$ and $N\sim 50$ provide unique opportunity to investigate the influence of $Z=38$,40 semimagic and $N=50$ magic shell gaps on the observed level structures especially at higher angular momentum. From this point, ^{92}Mo seemed to be an ideal candidate for such studies. The previous study on this nucleus was carried out using a moderate five Compton-suppressed HPGe detector array [2]. The authors did not observe fragmentation of intensity into parallel cascades after breaking of the $N=50$ core (around $14\hbar$). Similar phenomena, however, have been reported in the neighboring nuclei: for example, ^{94,95,96}Ru [1,7]

Hence, it seemed interesting to undertake an investigation of level structures at high spins for the $N=50$ nucleus $_{42}$Mo^{92} using a five Clover detector array, to look for the aforementioned features.

II. EXPERIMENTAL DETAILS AND ANALYSIS

Levels in ^{92}Mo were populated using a ^{74}Ge(^{28}Si,$2\alpha 2n$) reaction at an incident beam energy of 138 MeV. The ^{28}Si beam was provided by the 14 UD TIFR-BARC Pelletron facility at TIFR, Mumbai. An enriched ^{74}Ge target of 600 μg/cm^2 thickness backed by 10 mg/cm^2 Ta was used. The detector system employed for these measurements comprised of five Clover detectors together with a 14-element NaI(Tl) multiplicity filter. Among these, one of the Clover detectors had an anti-Compton shield. The detectors were placed at 15°, 30°, 45°, 70°, and 90° with respect to the beam direction in a planar geometry. The master trigger corresponded to a twofold event in the Clovers and a $K\geqslant 2$ condition, where K was the number of elements that had fired from the multiplicity filter. About 100×10^6 γ-γ coincident events were collected in the experiment. The list mode data were stored for a detailed off-line analysis. The data were sorted into conventional E_γ-E_γ matrices and analyzed using a Linux-based data sorting and data analysis program IUCSORT [8] and RADWARE [9]. From the background-subtracted gated spectra, 16 new γ transitions belonging to ^{92}Mo are identified and placed in a decay scheme using coincidence relationships and intensity arguments. Figure 1 illustrates a representative background-subtracted gated spectrum.

The γ-γ coincidences were also used to qualitatively assign the multipolarities of the observed transitions based on the intensity ratios extracted from angle-sorted matrices [10–12]. As described in Refs. [1,13,14] a γ-γ coincidence matrix was constructed with one axis corresponding to γ rays recorded by the 15° detector and the other axis corresponding to the γ rays recorded by the 70° detector. A gate corresponding to a γ ray of known multipolarity is taken for the detector on, say, the x axis and the coincident spectrum is

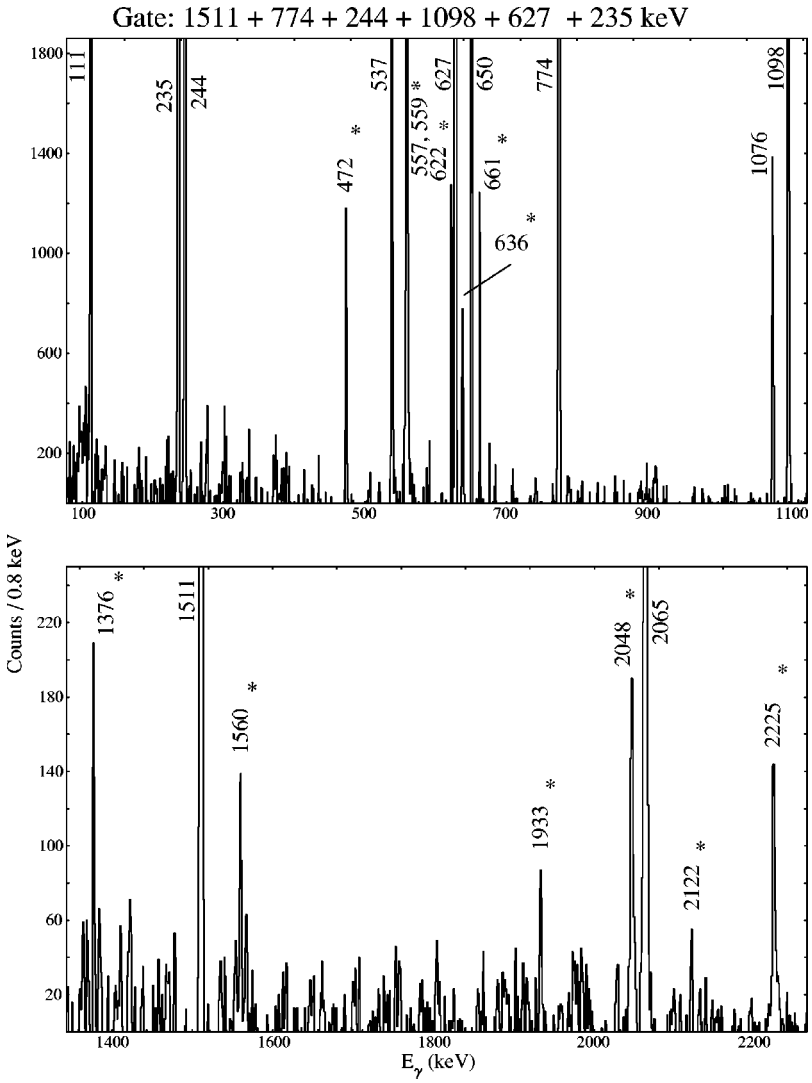

FIG. 1. γ-γ coincidence spectrum for ^{92}Mo with simultaneous gates on the 1511 keV ($2^+ \rightarrow 0^+$), 774 keV ($4^+ \rightarrow 2^+$), 1098 keV ($6^{(-)} \rightarrow 4^+$), 244 keV ($7^{(-)} \rightarrow 6^{(-)}$), 627 keV ($9^{(-)} \rightarrow 7^{(-)}$), and 235 keV ($11^{(-)} \rightarrow 9^{(-)}$) transitions. The energies are marked within ± 1 keV. The new transitions are indicated with an asterisk.

projected along the other axis. Next, the same gate is set on the y axis and the spectrum along the x axis is projected. Assuming the commonly encountered situation of stretched transitions, the intensities of transitions which have the same multipolarity as the gated γ ray remain approximately the same in both spectra. On the other hand, for γ rays with different multipolarities the intensities differ almost by a factor of 2. This is illustrated in Fig. 2 wherein the results (R_{int}) are obtained with sum gates of known quadruples.

The procedure described in Refs. [2,15] was also adopted to confirm our multipolarity assignments. This procedure is based on the observed angular distribution for dipole and quadrupole transitions, near 0° and 90° with respect to the beam axis. Two matrices were constructed with data from the 45° detector on the x axis and data from the 15° and 70° detectors on the y axis, respectively. We define R_{asym} as

$$R_{asym} = \frac{I_{\gamma_1} \text{ at } 70^\circ, \text{ gated with } \gamma_2 \text{ at } 45^\circ}{I_{\gamma_1} \text{ at } 15^\circ, \text{ gated with } \gamma_2 \text{ at } 45^\circ}.$$

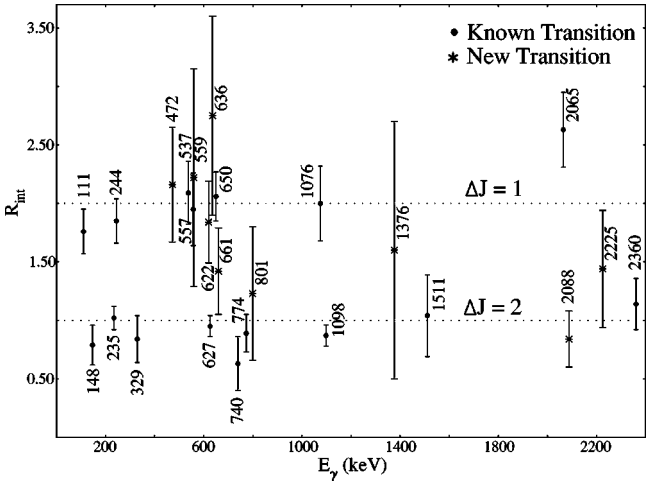

FIG. 2. γ-ray anisotropy intensity ratio R_{int} (see text), plotted against energies of γ-ray transitions in ^{92}Mo. The lines have been drawn to guide the eye. The quoted error includes the error due to background subtraction, fitting, and efficiency correction.

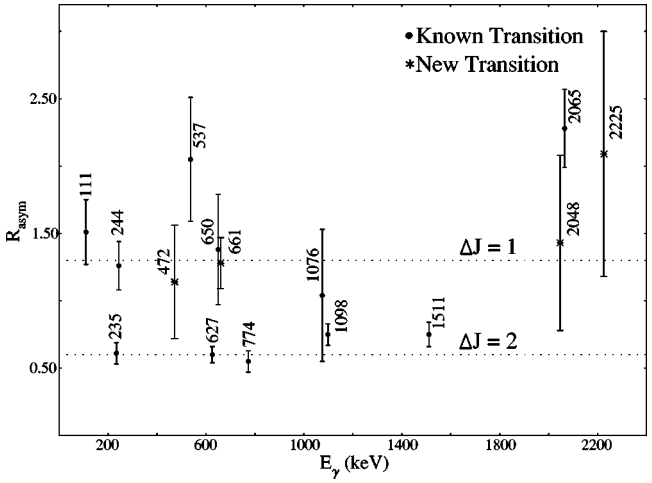

FIG. 3. Gamma-ray asymmetry R_{asym} plotted against energies of γ-ray transitions in ^{92}Mo. The lines have been drawn to guide the eye. Refer to the text for details. The quoted error includes the error due to background subtraction, fitting, and efficiency correction.

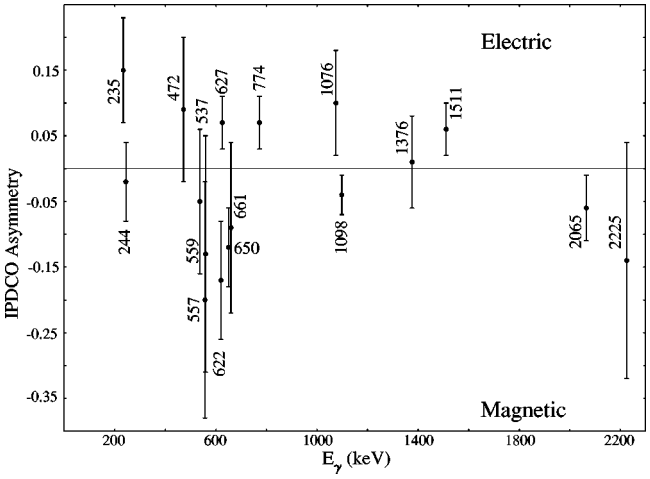

FIG. 5. Representative experimental gamma-ray asymmetry parameter, from polarization measurements plotted against energies of γ-ray transitions in ^{92}Mo. A positive value corresponds to an electric transition and a magnetic transition results in a negative value. The quoted error encompasses error due to background subtraction and fitting.

With this definition it was observed that for a quadrupole $R_{asym} \sim 0.6$ while for a dipole it was ~ 1.4 as seen in Fig. 3. All of the above assignments were based on the assumption that the observed transitions were stretched.

The use of a Clover detector facilitates polarization measurements which are crucial to determine the parity of the state involved with deexcitation of the transition studied. Each individual crystal of the Clover acts as scatterer and the two adjacent crystals as the absorber. Use of an array comprised of composite detectors such as Clovers facilitates coincidence polarization measurements [16–18]. This method has a unique advantage of reducing the contamination from neighboring nuclei and background, thereby helping in a more precise assignment for the parity of the excited state whose spin value is already known. Following the procedure suggested by Duchene *et al.* [16], the sensitivity of the Clover detector to the linear polarization of γ rays is illustrated in Fig. 4 by comparing the relative heights of the transitions in the summed perpendicular and parallel coincidence spectra. For an electric transition, a positive peak is observed in the difference between the perpendicular and parallel coincidences, whereas for a magnetic transition a positive peak is observed in the difference spectrum between the parallel and perpendicular spectra. For coincidence polarization measurements integrated polarizational-directional correlation from oriented nuclei (IPDCO) procedure was applied. The procedure is described in detail in Refs. [17,18]. Figure 5 illustrates the value of the asymmetry parameter. As seen from the figure a positive value indicates an electric nature whereas a negative value is associated with a magnetic nature. Admixtures would result in a near-zero value for the asymmetry parameter. Results obtained from the present statistics using a five Clover array are purely qualitative in nature.

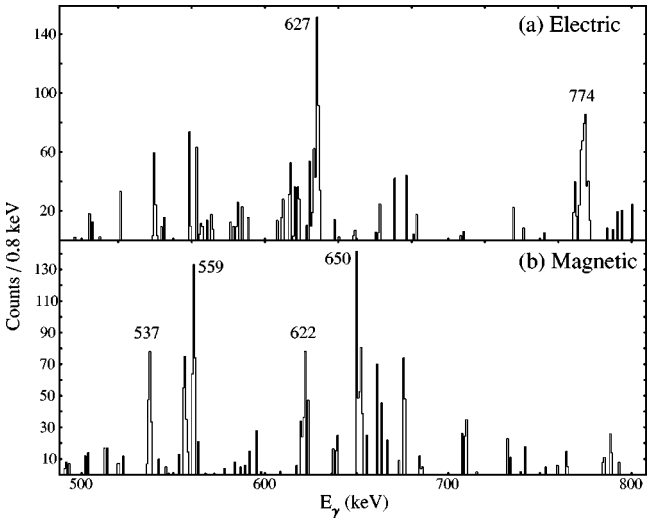

FIG. 4. Background-subtracted difference spectra for perpendicular minus parallel coincidences (a) and vice versa (b). The 627 and 774 keV transitions are of electric while the 537, 559, 622, and 650 are of magnetic character.

III. EXPERIMENTAL RESULTS

The identification of 16 new γ transitions has extended the level scheme up to an excitation energy of $E_x \sim 12$ MeV. The main observations in the present investigations are (a) presence of γ rays with $E_\gamma \sim 2$ MeV at spins around $14\hbar$. These are indicative of the breaking of the $N=50$ shell closure. (b) The presence of γ rays with $E_\gamma \sim 2$ MeV in the low-spin regime ($J \sim 8\hbar - 11\hbar$), a feature not reported in neighboring $N=50$ nuclei, viz., ^{93}Tc, ^{94}Ru. These originate due to excitation of protons across the Z

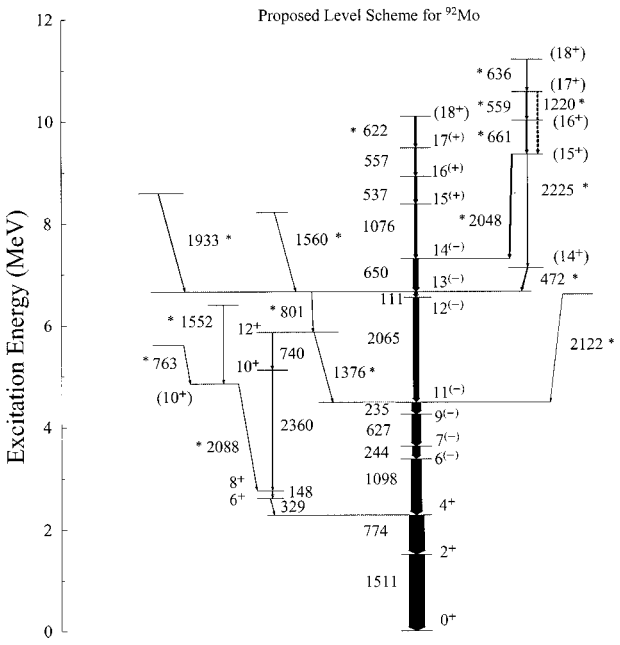

FIG. 6. Level scheme for ^{92}Mo for the levels populated in ^{74}Ge(^{28}Se,2α,$2n$)^{92}Mo reaction. Newly observed transitions are marked with an asterisk. The width of the arrows represents observed intensities. The spin and parity assignments, given in parentheses, are tentative.

$=38$ subshell closure. (c) Fragmentation of the intensity above $N=50$ core breaking.

The resultant level scheme for ^{92}Mo is illustrated in Fig. 6. The transition energies are marked within ± 1 keV. The width of the arrows are approximately equal to the intensities as obtained from the sum coincident spectra of the lowest two transitions, viz., 1511 keV ($2^+ \rightarrow 0^+$) and 774 keV ($4^+ \rightarrow 2^+$). The excitation energy (E_x), transition energy (E_γ), the relative intensity (I_γ), and the spin assignment of the observed γ rays in ^{92}Mo are summarized in Table I.

Singh *et al.* [2] assigned an electric character to both the 244 ($\Delta J=1$) and 1098 ($\Delta J=2$) keV transitions. Our multipolarity measurements confirm the $\Delta J=1$ and $\Delta J=2$ values for the 244 and 1098 keV transitions, respectively. Our polarization measurements for the 244 keV transition seem to indicate a possible admixture for its electromagnetic character. Assuming that the $E1$ assignment of the previous workers is correct, the transition would have a considerable $M2$ component. An $M2$ transition at such low energies would result in a long lifetime and therefore would be unobservable in the present study.

Hence, the $E1/M2$ nature for this transition is ruled out. The other possibility is that the 244 keV transition has a predominantly magnetic character, viz., $M1$ with some admixture from an $E2$ component, which could not be ascertained from the present data. In view of this, for the 244 keV transition a tentative $M1/E2$ assignment is suggested from the present study.

The 1098 keV transition involves change in angular momentum by 2 units and polarization measurements indicate a magnetic character. Assuming an $M2$ character for this transition the estimated lifetime would be typically about 1 ns, which is within our experimental time window for γ-γ coincidences. Thus, this transition has been assigned to have an $M2$ character.

Singh *et al.* [2] had assigned $J=5^-$ and 7^- spin and parity to levels ($E_x=2528$, $E_x=3626$ keV) deexciting via 244 and 1098 keV transitions. The 244 and 1098 keV transitions are now assigned an $M1$ and $M2$ character, respectively. Thus, the level at $E_x=2528$ keV would now have a spin and parity assignment of $J=5^+$ and the level at $E_x=3626$ keV would have a $J=7^-$ assignment. However, the shell model results discussed in the subsequent section predicted that the $J=5^+$ level would have an excitation energy of E_x

TABLE I. Gamma transition energy (E_γ) in keV, excitation energy (E_x) in keV, initial and final spins for the transitions, relative intensity (I_γ), and multipolarity of the transitions belonging to ^{92}Mo.

E_γ	E_x	$J_i^\pi \rightarrow J_f^\pi$	I_γ[a]	Mult.
110.7	6662	$13^{(-)} \rightarrow 12^{(-)}$	21.2(2.0)	$M1$
147.7	2761	$8^+ \rightarrow 6^+$	3.9(0.8)	$E2$
234.5	4487	$11^{(-)} \rightarrow 9^{(-)}$	55.0(6.0)	$E2$
243.8	3626	$7^{(-)} \rightarrow 6^{(-)}$	49.0(5.0)	$M1$
329.1	2613	$6^+ \rightarrow 4^+$	4.5(1.1)	$E2$
471.9	7134	$(14^+) \rightarrow 13^{(-)}$	7.2(1.7)	$E1$
537.1	8925	$16^{(+)} \rightarrow 15^{(+)}$	20.0(2.0)	$M1$
557.2	9482	$17^{(+)} \rightarrow 16^{(+)}$	13.3(2.2)	$M1$
559.2	10578	$(17^+) \rightarrow (16^+)$	7.8(1.9)	$M1$
621.9	10103	$(18^+) \rightarrow 17^{(+)}$	11.2(2.2)	$M1$
626.5	4252	$9^{(-)} \rightarrow 7^{(-)}$	61.0(6.0)	$E2$
636.3	11215	$(18^+) \rightarrow (17^+)$	6.4(2.0)	$M1$
649.7	7311	$14^{(-)} \rightarrow 13^{(-)}$	35.0(4.0)	$M1$
660.7	10019	$(16^+) \rightarrow (15^+)$	8.4(2.2)	$M1$
740.1	5862	$12^+ \rightarrow 10^+$	5.7(2.0)	$E2$
762.9	5612	$\rightarrow (10^+)$	3.0(1.0)	
773.7	2284	$4^+ \rightarrow 2^+$	100(13)	$E2$
800.7	6662	$13^{(-)} \rightarrow 12^+$	2.0(0.9)	$E1$
1075.7	8388	$15^{(+)} \rightarrow 14^{(-)}$	18.0(3.0)	$E1$
1097.9	3382	$6^{(-)} \rightarrow 4^+$	69.0(7.0)	$M2$
1220.0	10578	$(17^+) \rightarrow (15^+)$	w[b]	$E2$
1375.5	5862	$12^+ \rightarrow 11^{(-)}$	w[b]	$E1$
1510.5	1511	$2^+ \rightarrow 0^+$	100(3)	$E2$
1551.6	6400	$\rightarrow (10^+)$	w[b]	
1560.3	8222	$\rightarrow 13^{(-)}$	w[b]	
1933.2	8594	$\rightarrow 13^{(-)}$	w[b]	
2047.6	9359	$(15^+) \rightarrow 14^{(-)}$	10.0(1.0)	$E1$
2064.5	6551	$12^{(-)} \rightarrow 11^{(-)}$	39.0(4.0)	$M1$
2087.8	4849	$(10^+) \rightarrow 8^+$	2.9(0.8)	$E2$
2122.4	6608	$\rightarrow 11^{(-)}$	w[b]	
2224.5	9359	$(15^+) \rightarrow (14^+)$	5.3(1.9)	$M1$
2360.3	5121	$10^+ \rightarrow 8^+$	4.2(0.8)	$E2$

[a]The quoted errors on intensities encompass errors due to background subtraction, fitting, and efficiency correction.

[b]w indicates weak transitions whose intensity could not be computed.

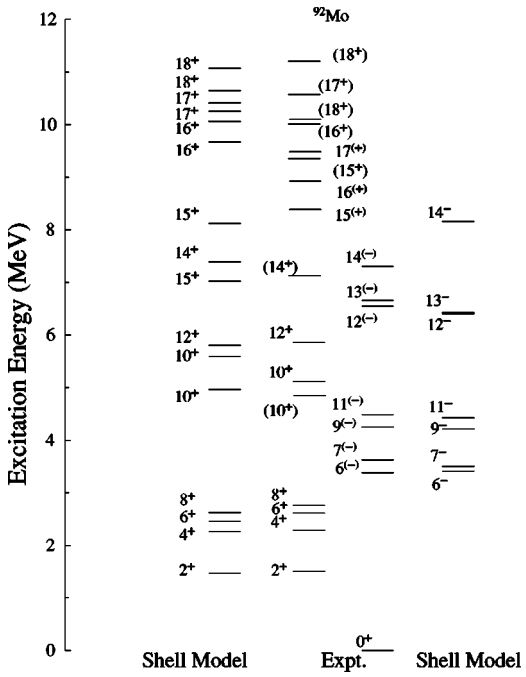

FIG. 7. Comparison of the observed states in ^{92}Mo with spherical shell model states.

$\sim$4500 keV, while the 7^- level is predicted at an excitation energy of $E_x \sim 3500$ keV. As seen from the shell model predictions, there is a large discrepancy between the observed excitation energy and the theoretical calculations for the $J=5^+$ level. However, if the placement of 244($M1$) and 1098($M2$) keV is interchanged, the resulting level now deexciting via the 1098 keV transition has a tentative spin and parity of $J=6^{(-)}$ and the excitation energy is $E_x=3382$ keV. The shell model predicts an excitation energy of 3480 keV for this level which is in reasonable agreement with the experimental value. Hence, the level deexciting via the 244 keV transition ($E_x=3626$ keV) has a spin and parity of $J=7^{(-)}$. Interchanging of the positions of 244 keV and 1098 keV gamma transitions is further supported by the intensity argument. The relative intensities of the 244 and 1098 keV transitions are 49(5) and 69(7), respectively, as seen from Table I. A similar intensity pattern was reported by Singh *et al.* [2].

The 1076 keV ($\Delta J=1$) transition was assigned an $M1$ character by earlier workers. The present data indicate that the 1076 keV transition involved a $\Delta J=1$ change in angular momentum and the polarization results suggest an electric nature. Thus, we have assigned it an $E1$ character, and the level at $E_x=8388$ keV is now tentatively assigned a spin and parity of $J=15^{(+)}$. The polarization measurements confirmed the magnetic nature for the earlier reported 537 and 557 keV transitions.

In the present studies 472($E1$), 559($M1$), 622($M1$), 636($M1$), 661($M1$), 763, 801($E1$), 1220($E2$) 1376($E1$), 1552, 1560, 1933, 2048($E1$), 2088($E2$), 2122, and 2225($M1$) γ rays belonging to ^{92}Mo nucleus were observed. The multipolarities were assigned using the procedure described in the earlier section. The position of the 801 and 1376 keV transitions helped to assign an $E1$ nature to both the transitions. The occurrence of a weak crossover transition, of energy 1220 keV(559+661 keV), supports a $M1$

TABLE II. Main partitions of the wave functions for ^{92}Mo. The wave function for a particular angular momentum state would be composed of several partitions, where each partition is of the form $P=[\pi(p(1),p(2),p(3),p(4))\otimes\nu(n(1),n(2),n(3))]$, where $p(i)$ represents the number of protons occupying the $f_{5/2}$, $p_{3/2}$, $p_{1/2}$, and $g_{9/2}$ orbits, and $n(j)$ represents the number of neutrons in the $p_{1/2}$, $g_{9/2}$, and $d_{5/2}$ orbits, respectively. In these calculations no neutrons were allowed to be excited to the $g_{7/2}$,$d_{3/2}$, and $s_{1/2}$, orbits.

J	Wave function	Seniority	Partitions
($\hbar$)	π	ν	%
0^+	$\pi(6,4,2,2)\otimes\nu(2,10,0)$	0	58.99%
	$\pi(6,4,0,4)\otimes\nu(2,10,0)$	0	19.84%
	$\pi(6,2,2,4)\otimes\nu(2,10,0)$	0	14.46%
2^+	$\pi(6,4,2,2)\otimes\nu(2,10,0)$	0	67.92%
	$\pi(6,4,0,4)\otimes\nu(2,10,0)$	0	15.41%
	$\pi(6,2,2,4)\otimes\nu(2,10,0)$	0	10.53%
4^+	$\pi(6,4,2,2)\otimes\nu(2,10,0)$	0	70.67%
	$\pi(6,4,0,4)\otimes\nu(2,10,0)$	0	14.50%
6^+	$\pi(6,4,2,2)\otimes\nu(2,10,0)$	0	70.25%
	$\pi(6,4,0,4)\otimes\nu(2,10,0)$	0	14.34%
8^+	$\pi(6,4,2,2)\otimes\nu(2,10,0)$	0	71.64%
	$\pi(6,4,0,4)\otimes\nu(2,10,0)$	0	14.63%
(10^+)	$\pi(6,4,0,4)\otimes\nu(2,10,0)$	0	57.68%
	$\pi(5,4,1,4)\otimes\nu(2,10,0)$	2	14.24%
	$\pi(4,4,2,4)\otimes\nu(2,10,0)$	0	13.68%
10^+	$\pi(5,4,1,3)\otimes\nu(2,10,0)$	3	73.88%
	$\pi(5,3,2,4)\otimes\nu(2,10,0)$	2	14.57%
12^+	$\pi(6,4,0,4)\otimes\nu(2,10,0)$	0	65.57%
	$\pi(6,3,1,4)\otimes\nu(2,10,0)$	2	10.28%
(14^+)	$\pi(5,4,1,4)\otimes\nu(2,10,0)$	2	71.42%
	$\pi(5,3,2,4)\otimes\nu(2,10,0)$	2	26.37%
$15^{(+)}$	$\pi(5,4,1,4)\otimes\nu(2,10,0)$	2	83.51%
	$\pi(5,3,2,4)\otimes\nu(2,10,0)$	2	14.11%
(15^+)	$\pi(6,4,2,2)\otimes\nu(2,9,1)$	2	83.41%
$16^{(+)}$	$\pi(5,4,1,4)\otimes\nu(2,9,1)$	4	98.39%
(16^+)	$\pi(5,4,1,4)\otimes\nu(2,9,1)$	4	99.09%
$17^{(+)}$	$\pi(5,4,1,4)\otimes\nu(2,9,1)$	4	99.45%
(17^+)	$\pi(5,4,1,4)\otimes\nu(2,9,1)$	4	96.05%
(18^+)	$\pi(5,4,1,4)\otimes\nu(2,9,1)$	4	99.20%
(18^+)	$\pi(5,4,1,4)\otimes\nu(2,9,1)$	4	96.39%
$6^{(-)}$	$\pi(5,4,2,3)\otimes\nu(2,10,0)$	2	51.44%
	$\pi(6,4,1,3)\otimes\nu(2,10,0)$	2	28.27%
$7^{(-)}$	$\pi(6,4,1,3)\otimes\nu(2,10,0)$	2	71.50%
	$\pi(5,4,2,3)\otimes\nu(2,10,0)$	2	12.35%
$9^{(-)}$	$\pi(6,4,1,3)\otimes\nu(2,10,0)$	2	79.97%
	$\pi(6,3,2,3)\otimes\nu(2,10,0)$	2	11.68%
$11^{(-)}$	$\pi(6,4,1,3)\otimes\nu(2,10,0)$	2	86.16%
$12^{(-)}$	$\pi(5,4,2,3)\otimes\nu(2,10,0)$	2	82.34%
$13^{(-)}$	$\pi(5,4,2,3)\otimes\nu(2,10,0)$	2	73.70%
	$\pi(5,4,0,5)\otimes\nu(2,10,0)$	2	12.02%
$14^{(-)}$	$\pi(6,4,1,3)\otimes\nu(2,9,1)$	4	62.44%
	$\pi(6,3,2,3)\otimes\nu(2,9,1)$	4	20.24%
	$\pi(5,4,2,3)\otimes\nu(2,9,1)$	4	14.89%

multipolarity to both the 661 keV and 559 keV transitions and an $E2$ multipolarity to the 1220 keV transition simultaneously. The multipolarity assignment procedure for the 472 keV γ ray indicated a $\Delta J=1$ transition. The polarization measurements indicated an electric character for this transition. Further the other members of the sequence, viz., 636-559-661-2225 keV transitions, had a $\Delta J=1$ change in angular momentum and a similar polarization different than that observed for the 472 keV transition. Hence, tentatively an $E1$ character to the 472 keV γ ray is assigned and an $M1$ character to all the other in-band members of this sequence. Assuming that the 472 keV is an $E1$ transition the level at 7134 keV excitation energy has a tentative spin and parity assignment of $J=(14^+)$; shell model calculations predicted an excitation energy of 7388 keV and 8161 keV for the $J=14^+$ and the $J=14^-$ levels, respectively. Thus the present shell model calculations support the $E1$ nature of the 472 keV transition. The assignment of a positive parity to levels deexciting via the 636-559-661-2225-472 cascade was supported by our shell model calculations.

In addition to these a 1902 keV transition is also observed in the present study, which could not be placed in the level scheme within the present statistics.

IV. THEORETICAL DISCUSSIONS

Shell model calculations have been carried out using the code OXBASH [19]. The model space utilized in the calculation includes four proton orbits $(f_{5/2},p_{3/2},p_{1/2},g_{9/2})$ and six neutron orbits $(p_{1/2},g_{9/2},g_{7/2},d_{5/2},d_{3/2},s_{1/2})$. This model space was code named GWB in the code OXBASH [19]. It has ^{66}Ni ($Z=28$, $N=38$) as the inert core. Since an empirical Hamiltonian for this configuration is not available, it was necessary to use a combination of empirical Hamiltonians along with experimental values for the two-body matrix elements. The details of the two-body matrix elements used are given in Ref. [5].

Because of the large number of active orbitals, a truncation of model space is necessary to make the calculations feasible. The model space could be internally truncated by performing the calculations for the most dominant configurations [5]. It is expected that states up to $J=10\hbar-12\hbar$ could be described by the redistribution of the valence protons in the *fpg* subspace, and the neutron core may be assumed to be inert [4]. The excitation of the neutron core is essential for the description of only the higher-angular-momentum states $(J\geqslant 12\hbar-14\hbar)$. Details of such calculations are given in Ref. [5].

The presence of γ rays with $E_\gamma\sim 2$ MeV is an indication of the excitation of nucleons across a large energy (shell) gap. The occurrence of $E_\gamma\sim 2$ MeV at $(J\sim 14\hbar)$ is an indication of the excitation of neutrons across the $N=50$ shell closure. However, the presence of such large energy γ transitions at low spins $(J\sim 8\hbar-11\hbar)$ could be attributed to the excitation of protons across the $Z=38$ subshell gap. For these states we have performed the calculations by incorporating both the above-mentioned configurations originating from the proton excitation across the $Z=38$ gap and the neutron excitation across the $N=50$ shell closure.

Figure 7 illustrates the comparison between the experimental excitation energies and the theoretical predictions of the spherical shell model calculations. Table II summarizes these shell model calculations.

As seen from the table, even the ground state has about a 10% contribution from the configuration arising due to excitation of protons across the $Z=38$ subshell closure. Hence, the $\pi(p_{1/2},g_{9/2})$ model space would be inadequate to describe even the low-lying levels in this $N=50$ nucleus. As mentioned above, states with $J\leqslant 8^+,9^-$ are dominated by excitation of the valence protons within the $\pi(p_{1/2},g_{9/2})$ orbitals. States with $8^+,9^-\leqslant J\leqslant 12^+,13^-$ are dominated by excitation of the protons from the $(f_{5/2},p_{3/2})$ to $(p_{1/2},g_{9/2})$ orbitals. For these states it is found that the wave function is dominated by the $\pi(f_{5/2},p_{3/2})^{(-1)}$ configurations coupled to the proton excitations in the $p_{1/2},g_{9/2}$ orbitals with an inert $N=50$ neutron core. The states with $J\geqslant 14\hbar$ arise due to the neutron-particle-hole excitation across the $N=50$ shell closure, coupled to the valence-proton configurations within the *fpg* valence space.

The shell model calculations indicate single-particle behavior of the level structure up to the highest observed spins and excitation energies.

V. SUMMARY

The level structure of the $N=50$ nucleus ^{92}Mo at high spins produced in the ^{28}Si+^{74}Ge fusion reaction has been deduced. A five Clover array was used to detect the deexciting γ rays.

Sixteen new transitions belonging to this nucleus have been identified and placed in the decay scheme. Assignments of spin and parity for most of the excited states were carried out using DCO and IPDCO methods. The level scheme is now extended up to an excitation energy of $E_x\sim 11$ MeV and spins up to $J=18\hbar$.

The resulting level scheme is compared with large basis shell model calculations. The two are in reasonable agreement with each other.

The highlight of the present investigation is the identification of levels arising from the excitation of the $Z=38$ subshell closure and the $N=50$ shell closure.

However, additional spectroscopic data such as lifetimes and polarizational correlation measurements will help an unambiguous assignment of the underlying intrinsic microscopic configurations for this $N=50$ nucleus.

ACKNOWLEDGMENTS

The help received from the accelerator staff at BARC-TIFR, Pelletron, Mumbai is gratefully acknowledged. The authors would like to thank Dr. S. K. Basu for several helpful discussions. Two of the authors (N.S.P., S.S.G) would like to thank their colleagues at IUC-DAEF,CC for their cooperation during the target preparations and in the course of data analysis.

[1] S.S. Ghugre, S.B. Patel, M. Gupta, R.K. Bhowmik, and J.A. Shiekh, Phys. Rev. C **50**, 1346 (1994).
[2] Pragya Singh, R.G. Pillay, J.A. Sheikh, and H.G. Devare, Phys. Rev. C **45**, 2161 (1992).
[3] H.A. Roth, S.E. Arnell, D. Foltescu, O. Skeppstedt, J. Blomqvist, A. Nilsson, T. Kuroyanagi, S. Mitarai, and J. Nyberg, Phys. Rev. C **50**, 1330 (1994).
[4] Xiandong Ji and B.H. Wildenthal, Phys. Rev. C **37**, 1256 (1988); **38**, 2849 (1988).
[5] S.S. Ghugre and S.K. Datta, Phys. Rev. C **52**, 1881 (1995).
[6] D. Rudolph, K.P. Lieb, and H. Grawe Nucl. Phys. **A597**, 298 (1996).
[7] B. Kharraja, S.S. Ghugre, U. Garg, R.V.F. Janssens, M.P. Carpenter, B. Crowell, T.L. Khoo, T. Lauritsen, D. Nisius, W. Reviol, W.F. Mueller, L.L. Riedinger, and R. Kaczarowski, Phys. Rev. C **57**, 83 (1998).
[8] N. S. Pattabiraman, S. S. Ghugre, and S. N. Chintalapudi, Proceedings of the DAE Symposium on Nuclear Physics, 2000, Vol. 43B, p. 207.
[9] D.C. Radford, Nucl. Instrum. Methods Phys. Res. A **361**, 297 (1995).
[10] K.S. Krane, R.M. Steffen, and R.M. Wheeler, Nucl. Data Tables **11**, 351 (1973).
[11] A. Kramer-Flecken, T. Morek, R.M. Lieder, W. Gast, G. Hebbinghaus, H.M. Jager, and W. Urban, Nucl. Instrum. Methods Phys. Res. A **275**, 333 (1989).
[12] L. Peter Ekstrom and Anders Nordlund, Nucl. Instrum. Methods Phys. Res. A **313**, 421 (1992).
[13] F.S. Stephens, M.A. Delenplanque, R.M. Diamond, A.O. Macchiavelli, and J.E. Draper, Phys. Rev. Lett. **54**, 2584 (1985).
[14] C.W. Beausang, D. Prévost, M.H. Bergström, G. de France, B. Haas, J.C. Lisle, Ch. Theisen, J. Timár, P.J. Twin, and J.N. Wilson, Nucl. Instrum. Methods Phys. Res. A **364**, 560 (1995).
[15] H. Harada, M. Sugawara, H. Kusakari, H. Shinohara, Y. Ono, K. Furuno, T. Hosoda, M. Adachi, S. Matsuki, and N. Kawamura, Phys. Rev. C **39**, 132 (1989).
[16] G. Duchene, F.A. Beck, P.J. Twin, G. de France, D. Curien, L. Han, C.W. Beausang, M.A. Benteley, P.J. Nolan, and J. Simpson, Nucl. Instrum. Methods Phys. Res. A **432**, 90 (1999).
[17] Ch. Droste, K. Starosta, A. Wierzchucka, T. Morek, S.G. Rohozinskii, J. Srebrny, M. Bergstrom, B. Herskind, and E. Wesolowski, Nucl. Instrum. Methods Phys. Res. A **337**, 430 (1999).
[18] K. Starosta, T. Morek, Ch. Droste, S.G. Rohozinskii, J. Srebrny, A. Wierzchucka, M. Bergstrom, B. Herskind, E. Melby, T. Czosnyka, and P.J. Napiorkowski, Nucl. Instrum. Methods Phys. Res. A **423**, 16 (1999).
[19] B.A. Brown, A. Etchegoyen, W.D.M. Rae, and N.S. Godwin computer code OXBASH, 1984.